10-14 July 2016, Vienna, Austria

Coupled CFD-PBE Predictions of Renal Stone Size Distributions in the Nephron in Microgravity

Mohammad Kassemi [1] Elise Griffin[2], and David Thompson[3]

National Center for Space Exploration Research
NASA Glenn Research Center
Cleveland, OH, 44139

In this paper, a deterministic model is developed to assess the risk of critical renal stone formation for astronauts during space travel. A Population Balance Equation (PBE) model is used to compute the size distribution of a population of nucleating, growing and agglomerating renal calculi as they are transported through different sections of the nephron. The PBE model is coupled to a Computational Fluid Dynamics (CFD) model that solves for steady state flow of urine and transport of renal calculi along with the concentrations of ionic species, calcium and oxalate, in the nephron using an Eulerian two-phase mathematical framework. Parametric simulation are performed to study stone size enhancement and steady state volume fraction distributions in the four main sections of the nephron under weightlessness conditions. Contribution of agglomeration to the stone size distribution and effect of wall friction on the stone volume fraction distributions are carefully examined. Case studies using measured astronaut urinary calcium and oxalate concentrations in microgravity as input indicate that under nominal conditions the largest stone sizes developed in Space will be still considerably below the critical range for problematic stone development. However, results also indicate that the highest stone volume fraction occurs next to the tubule and duct walls. This suggests that there is an increased potential for wall adhesion with the possibility of evolution towards critical stone sizes.

Nomenclature

B^o	=	nucleation rate
D	=	particle diameter
$D_{j,m}$	=	mass diffusion coefficient of species j in urineG_D = linear growth rate
G_v	=	volumetric growth rate
K_b	=	nucleation rate constant
K_g	=	growth rate constant
$\dot{m}_{p,q}$	=	mass transfer rate from p^{th} phase to q^{th} phase
n	=	particle population density
N	=	particle number density
p	=	pressure
R	=	particle radius
R_{pq}	=	momentum interaction force between p^{th} and q^{th} phases
RS	=	relative supersaturation of calcium oxalate in urine
S	=	supersaturation of calcium oxalate in urine
t	=	time
$\vec{u}$	=	velocity vector
h	=	height

[1] Chief Scientist, National Center for Space Exploration Research, NASA Glenn Research Center, 21000 Brookpark Rd, MS110-3 Cleveland, OH 44135.
[2] NSBRI Intern, Currently at Department of Mathematics, Utah State University, Ogden, Utah.
[3] USRA Research Associate, National Center for Space Exploration Research, NASA Glenn Research Center, 21000 Brookpark Rd, MS105-1 Cleveland, OH 44135

Y_j = mass fraction of species j
t = time

Greek

α = volume fraction
β = particle agglomeration kernel
ρ = density
$\bar{\bar{\tau}}$ = stress-strain tensor

Subscripts

Ca = calcium
Ox = oxalate
p = p^{th} phase that transfers mass
q = q^{h} phase that receives mass
j = species inde
1 = pertaining to urine
2 = pertaining to Calcium Oxalate

I. Introduction

The risk of astronauts developing kidney stones is a serious concern for NASA, especially, since the duration of future space expeditions will be substantially increasing. The concern seems to be justified since a recent survey of renal stone formation in US astronauts has revealed 14 recorded episodes[1]. Several incidents occurred in the preflight period (n=5) while other episodes (n=9) were in the post flight phase. The time period for the onset of symptomatic stone formation following return to earth ranged from 9-120 months after landing. Six out of the nine post-flight episodes occurred after 1994, which corresponded with the extension of the shuttle missions to 12 days.

Renal stones come in different types and the formation of a specific stone-type usually depends upon the existence of particular risk factors that are often revealed by the subject's 24-hr urine biochemical analysis. Nevertheless, the most common renal stone and a main component in stones of mixed composition is calcium oxalate (CaOx). It accounts for almost 85% of the clinical occurrences of nephrolithiasis. Four out of the six kidney stones of known composition developed by the astronauts have also been calcium oxalate[2].

Space travel has a profound impact on the nephron biochemistry. Due to bone atrophy[1-3] and lower urine volumes caused by dehydration[4-5], concentration of both calcium (Ca) and oxalate (Ox) and hence the urinary supersaturation of CaOx can become significantly elevated. There are other contributing factors such as the astronauts' high protein and sodium level that in addition to inducing higher calcium and pH levels can also provide nidi that may serve as nucleation sites thus promoting CaOx precipitation[5-6]. The higher pH levels will also lower the concentration of citrate one of the primary inhibitors of CaOx growth and agglomeration[6-7]. In short, alterations in the renal biochemistry of astronauts tend to provide favorable conditions for increased nucleation, growth, and agglomeration of CaOx stones in the renal system.

Because of the considerable danger that a clinically significant renal stone incident can pose to the astronauts' health and to the success of future missions, NASA has focused on using both pro babilistic[8] and deterministic[9] computational models to assess the risks of renal colic for various mission scenarios. To address this need, in the present work, we have developed for the first time a comprehensive model for renal stone formation and transport through the nephron. This is accomplished by coupling the Population Balance Equation (PBE) for nucleation, growth and agglomeration of renal calculi to a Computational Fluid Dynamics (CFD) model that solves for flow of urine and transport of renal calculi along with the concentrations of the ionic species, calcium and oxalate, using a Eulerian two-phase mathematical framework.

CaOx stone development has been subject to various theoretical considerations; both in isolation[10, 11] and in the context of its passage through the renal system[12-16]. The physical mechanisms that govern nucleation and crystal growth are relatively well known and have been subject to a comprehensive monograph by Nielsen and Christoffersen[11] respectively. A coupled kinetics-transport treatment of CaOx crystal precipitation has been presented by Kassemi et al.[10] where special attention is devoted to urinary stone formation.

Finlayson[12] was the first to consider the ducts of Bellini and the pelvis as a system of continuous crystallizers in series and applied a mixed suspension mixed product removal (MSMPR) analysis similar to the ones employed

extensively in chemical reactor engineering to predict the size distributions for a population of nucleating and growing crystals. Subsequently, Finlayson and Reid[13] and later Kavanagh[14] concluded that in order for the calculi to become large enough to cause blockage, some kind of particle fixation or retention such as wall adhesion must take place. This became known as the *fixed particle* concept[13]. Finlayson's analysis, however, considered only nucleation and growth and neglected the important effects of agglomeration.

Roughly two decades after Finlayson's *fixed-particle* concept, Kok and Khan[15] used more appropriate data for the tubular dimensions and accounted for particle agglomeration, albeit, in a quite simplified manner to show that tubular blockage may be possible even without particle fixation when agglomeration is taken into account. This has come to be known the *free-particle* concept. Robertson[16] complemented the previous theoretical treatments of the problem by considering the effects of tube wall, fluid drag and gravity and concluded that there is still a possibility that wall drag and gravity may delay the passage of stones travelling close to the tubule walls to an extent that they would grow large enough to cause obstruction.

Although the precise mechanisms for kidney stone formation and growth are still not well-understood, recent studies by Kim et al.[17] and Evan at al.[18] using advanced endoscopic imaging and comprehensive physiological biopsies suggest three possible free/fixed pathways to stone formation: (a) nucleation and growth on the Randall plaque deposits in the papillae; (b) growth after adherence to a possibly injured section of collecting or Bellini ducts; (c) homogeneous nucleation and growth in the urine during passage through the nephron. The Randall plaque overgrowth mechanism seems to be the most common pathway for CaOx stone development in idiopathic stone formers.

In the present work, we have assumed that regardless of where the stone formation originates it is accomplished through the three coupled mechanisms of nucleation, growth and agglomeration as described by the Population Balance Equation[19, 20]. Using a coupled PBE-CFD model, we study the evolution of steady state renal calculi size and volume fraction distributions under microgravity conditions in the four segments of the nephron, namely: the proximal tube; the descending and ascending tubes of Henle; the distal tube; the upper and lower collecting ducts; and finally the duct of Bellini. The impact of flow and transport on the volume fraction distributions in the renal tubules and ducts is carefully examined. It is shown that for the first two nephron segments, a mixed-suspension mixed-product removal (MSMPR) continuous crystallizer model as adopted by many of the previous theoretical work is not valid. The important impact of agglomeration on renal stone size distributions are also discussed.

II. Mathematical Model

Urine flows through the kidney through a cascading system of interconnected nephron tubules and ducts. There are about 1,200,000 tubules connecting to 200,000 outer medullary collecting ducts (OMCD) emptying into 512 inner medullary collecting ducts (IMCD) that finally lead into 32 ducts of Bellini (DoB). So in one branch of nephron there are 6 tubules connected to each OMCD, 39 OMCDs connected to each IMCD, and 16 IMCDs per duct of Bellini. The tubule segment itself consists of 4 sections: the proximal tube, the descending tube of Henle, the ascending tube of Henle and the distal tubule. For a nominal 1.44 liter/day urine excretion rate, Kok and Kahn[15], have calculated the net urinary flow rates through each of the 4 main nephron sections based on their corresponding conduit diameters and re-absorption rates. This information is presented in Table 1 and is used to construct the computational model for each of the four main nephron segments.

An Eulerian approach is adopted to capture the two phase stone-urine flow through each segment of the nephron, within the framework of the Ansys/Fluent CFD code[21]. According to this approach, the transport of urine and stone in the nephron is subject to the following two phase continuity and momentum equations:

$$\frac{\partial}{\partial t}\left(\propto_q \rho_q\right) + \nabla \cdot \left(\propto_q \rho_q \vec{u}_q\right) = \sum_{p=1}^{2}\left(\dot{m}_{pq} - \dot{m}_{qp}\right) \quad (1)$$

Table 1. Dimensions, flow rates, and computational grids for the four nephron segments

Nephron Section	Length (mm)	Diameter (microns)	Net Volumetric Flow Rate (m^3/s)	Number of Flow Cells	Number of PBE Particle Size Bins
Tubule	40	25	$8.06(10)^{-14}$	60000	36
IMCD	16	33	$1.55(10)^{-13}$	24000	36
OMCD	6	40	$5.40(10)^{-12}$	16511	41
DoB	5	80	$2.72(10)^{-11}$	21267	50

$$\frac{\partial}{\partial t}\left(\propto_q \rho_q \vec{u}_q\right) + \nabla \cdot \left(\propto_q \rho_q \vec{u}_q \vec{u}_q\right) = -\alpha_q \nabla p + \nabla \cdot \bar{\bar{\tau}}_q + + \sum_{p=1}^{2}\left(\overrightarrow{R_{pq}} + \dot{m}_{pq}\vec{u}_{pq} - \dot{m}_{qp}\vec{u}_{qp}\right) \quad (2)$$

In the above equations subscript, $q = 1$ represents the urine fluid phase and, $q = 2$ represents the CaOx stone phase. The volume fractions, α_q, is subject to, $\alpha_1 + \alpha_2 = 1$. $\vec{u}_q$ is the velocity of phase, q, and, $\dot{m}_{pq}$, characterizes the mass transfer from the p^{th} phase to the q^{th} phase. The q^{th} phase stress strain tensor is given by, $\bar{\bar{\tau}}_q$, and, $\overrightarrow{R_{pq}}$, is the interphase momentum interaction force on phase, q, as described in detail in reference 21. The interphase velocities,$\vec{u}_{pq}$, are defined as follows: if $\dot{m}_{pq} > 0$, that is phase p mass is transferred to phase q, then, $\vec{u}_{pq} = \vec{u}_p$; If $\dot{m}_{pq} < 0$, then $\vec{u}_{pq} = \vec{u}_q$. Similarly, if $\dot{m}_{qp} > 0$, then $\vec{u}_{qp} = \vec{u}_q$ and if $\dot{m}_{qp} < 0$, then $\vec{u}_{qp} = \vec{u}_p$.

As renal calculi nucleate and grow, urinary calcium and oxalate are used up to feed the precipitation process. Thus, the more crystals are formed, the larger will be the extent of calcium and oxalate depletion in the urinary flow. Transport of urinary Ca and Ox through the nephron is described by the species conservation equation that is written for the two ionic species as:

$$\frac{\partial}{\partial t}\left(\propto_1 \rho_1 Y_j\right) + \nabla \cdot \left(\propto_1 \rho_1 \vec{u}_1 Y_j\right) = \nabla \cdot \alpha_1 \rho_1 D_{j,m} \nabla Y_j - \dot{m}_{12} Y_j \qquad \text{for} \quad j = \text{Ca, Ox} \quad (3)$$

We assume that within the Eulerian two-phase system described by Eqs. 1-3 for the nephron, renal calculi form and develop through the three coupled mechanisms of nucleation, growth (precipitation) and agglomeration. This process can be described by the Population Balance Equation (PBE) for the CaOx particles as follows[20]:

$$\frac{\partial n(v)}{\partial t} + \nabla \cdot [\vec{u}_2 n(v)] + \nabla_v \cdot [G_v n(v)] = \int_0^v \beta n(v - Dv') n(v') dv' - n(v) \int_0^\infty \beta n(v') dv' \quad (4)$$

In the above equation, n (v) is the volume based population balance density with, v, as the crystal volume. In this analysis the agglomeration kernel, β , is assumed to be constant and independent of the particle diameter. Assuming spherical particles, the volumetric growth rate, G_v, in Eq. (4) can be written in terms of the linear growth rate, G_D, as:

$$G_v = 2\pi R^2 G_D \quad (5)$$

Due to nucleation, Eq. (1) is subject to an initial condition which can be written in terms of the nucleation rate,B^o for the nidus or zeroth size as:

$$n\,(v = 0) = n^o = {B^o}/{G_D} \quad (6)$$

The growth and nucleation rates in Eq. (4-6) are given by[9-11, 22-23]:

$$G_D = = K_g\{RS - 1\}^2 = K_g S^2 \quad (7)$$

$$B^o = K_b\{RS - 1\}^{2.88} = \quad K_b S^{2.88} \quad (8)$$

Where it is assumed that the growth of the crystal is limited by the kinetics of the 2[nd] order reaction[10]. Here, S and RS, are respectively the supersaturation and relative supersaturation of calcium oxalate in the urine and, K_g, and, K_b, are the growth and nucleation rate constants, respectively.

The PBEs (4-8) are coupled to the Eulerian two-phase conservation equations (1-3) for CaOx and urine through the total volume fraction of the CaOx stones, $\propto_2$ in Eqs. (1-2) and by the interphase mass transfer term,$\dot{m}_{12}$, in Eqs. (1) and (3). The stone volume fraction is calculated by integrating the population density, n(v), over the entire particle size range, that is:

$$\alpha_2 = \int_0^{v_{max}} n(v) v dv \quad (9)$$

Similarly, the interphase mass transfer rate from urine to stone,$\dot{m}_{21}$, is evaluated as:

$$\dot{m}_{12} = \rho_1 \frac{\alpha_1}{\alpha_2} \int_0^\infty \frac{\pi}{2} G_v(v) n(v) dv \quad (10)$$

Equations (1-10) constitute the system of governing equations that have to be solved numerically for the steady state velocities, concentrations, volume fractions, and population densities. The main inputs to the model are listed in Table 2.

Table 2. Physiochemical inputs to the model

Physio-Chemical Properties	Nominal Values	Reference
C_{Ca} (moles/L)	$3.27\ (10)^{-3}$	[24]
C_{Ox} (moles/L)	$2.41(10)^{-4}$	[24]
K_g (m/s)	$5.90\ (10)^{-10}$	[23,27]
K_b (1/m^3-s)	$5.90(10)^{7}$	[13,23]
β (m^3/s)	$2.78\ (10)^{-14}$	[23]
D_{nidus} (m)	$5\ (10)^{-7}$	
α_{inlet}	10^{-8}	
ρ_1 (kg/m^3)	1016	[28]
ρ_2 (kg/m^3)	2200	[13]
μ_l (Pa-s)	$8.3(10)^{-5}$	[28]
$D_{j\text{-}m}$ (m^2/s)	$1(10)^{-9}$	[29]

It is important here to note that the present mathematical model is subject to three important simplifying assumptions. First is with regard to the linear growth rate that is taken to be independent of stone dimension/radius. In general the growth rate of the crystal depends on the ionic activities of Ca and Ox at the growth surface that, in turn, is governed by a coupled competition between the supply of the ionic species by transport and incorporation of the ions into the crystal by the precipitation reaction. Since transport is dependent on diameter of the crystal, the growth rate is also in general size dependent. But for calcium oxalate, the precipitation reaction rate is very small compared to the transport rate especially for smaller stone sizes. Kassemi et al.[10] have described the interaction between species transport and reaction kinetics and its effect on the growth rate. They have shown that for the case here, where the stone diameters are below 1 mm, it is justified to assume that the growth rate is limited by the slow deposition reaction of the ionic salt. Under these circumstances the ionic activities of calcium and oxalate at the surface of the crystal approach their bulk urinary values and thus the growth rate becomes independent of crystal size.

Second, in this analysis it is assumed that the nephron segments can be represented by straight axisymmetric tube/duct sections. While this is a good assumption for the collecting ducts, it is less valid for the tubule segment that has a complex convoluted 3D geometry. Finally, the present analysis uses net uniform volumetric flow rates through each of the nephron segments and uniform urinary concentrations of Ca and Ox that are taken from the average 24hr urine sample analyses of the astronauts on the day of landing[24]. While these concentrations are not constant and change due to urinary depletion that feeds the crystallization process, the changes in Ca and Ox concentration along the nephron due to the filtration-reabsorption processes are not considered.

III. Numerical Implementation

The governing equations (1)–(10) for renal stone formation and transport are solved using a customized version of ANSYS/Fluent CFD code[21] where the crystal growth and nucleation models are incorporated via in-house supplied User Defined Functions (UDF)s. Simulations are performed for the four sections of nephron assuming axisymmetric geometry and boundary conditions and a laminar urinary flow. All the physiochemical and material properties are assumed to be constant. Volume weighted mixing laws are used in the species equations.

For the parametric case studies presented in the next section, steady state solutions are generated for each of the four nephron segments described previously, starting first with the tubule section and ending with the DoB segment. Uniform volume fraction of particles at the nidus size and uniform urinary calcium and oxalate concentrations are supplied at the inlet of the tubule segment. For each subsequent segment the area-averaged stone volume fraction, particle size distribution, and Ca and Ox concentrations obtained at the outlet of the previous segment are used together with the flow rates listed in Table 1 as inlet boundary condition. Since as mentioned before, net urinary flow rates are used in the present analysis and the filtration-reabsorption process is not modelled, the walls of the nephron segments are assumed to be impermeable and subject to nonslip velocity condition.

As indicated in Table 1, graded computational grids with 60,000, 24,000, 16,511, and 21,267 flow cells are used respectively for the tubule, IMCD, OMCD and DoB sections for flow, volume fraction and concentration discretization. For the PBE system, the volume coordinate is discretized into a graded series of bin sizes based on a logarithmic scale with; $\frac{v_i}{v_{i+1}} = 2^s$, where s is the volume bin ratio factor. The number of volume bins used for the tubule, IMCD, OMCD, and DoB segments are respectively, 36, 36, 41, and 50. For each nephron segment, the first

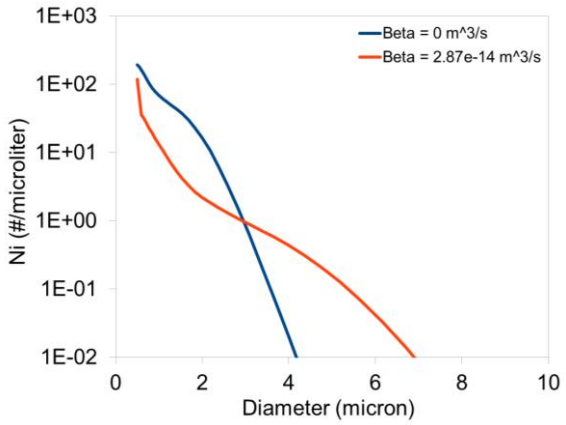

Figure 1. Volume integrated CaOx number density as function of diameter for non-agglomeration and agglomeration cases in the tubule segment.

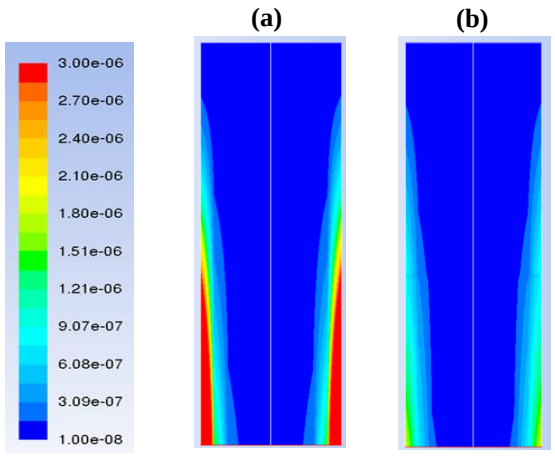

Figure 2. CaOx volume fraction distribution in the tubule segment: (a) β = 0; (b) β = 2.5(10)$^{-14}$ m^3/s. Figure is not to scale.

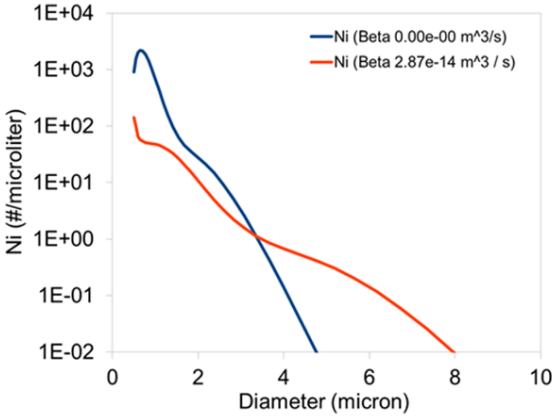

Figure 3. Volume integrated CaOx number density as function of diameter for non-agglomeration and agglomeration cases in the IMCD segment.

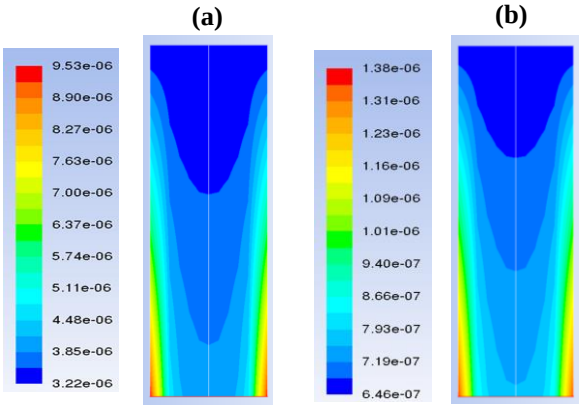

Figure 4. CaOx volume fraction distribution in the IMCD segment: (a) β = 0; (b) β = 2.5(10)$^{-14}$ m^3/s. Figure is not to scale.

(smallest) bin volume corresponds to the nucleation or nidus size with a diameter of 5 (10)$^{-7}$ m. A bin ratio factor of, $s = 0.375$, is used for all four nephron segments.

Steady state CFD solutions for each of the four segments were arrived at using a pseudo-transient time stepping scheme based on a robust implicit coupled pressure-velocity algorithm customized for the present Eulerian analysis. The PBEs, are solved using a volume discretization scheme based on the work by Hounslow and company[25, 26]. A second order monotone upwinding scheme is used to discretize the convective fluxes in the continuity, momentum, and species equations. A Least Squares Cell Based scheme is employed for the gradient calculations (cell face values). A modified High Resolution Interface Capturing (HRIC) scheme is adopted for tracking the volume fractions.

Point Implicit (Gauss-Seidel) linear equation solver with Algebraic Multi-Grid (AMG) method is used to solve the linearized systems of discretized equations. A tight convergence criterion of 10^{-5} is employed for all the variables. To optimize run times and increase numerical convergence rates, appropriate relaxation factors are applied to the main degrees of freedom in the momentum and species equations and individually optimized pseudo-time-step factors are designated for the different bin volume fractions.

Due to absence of any appropriate in-vitro renal stone experiments and lack of pertinent in-vivo data under controlled and definable conditions, experimental validation of the present model is not possible at this time. However, the PBE model used in the present analysis has been previously verified and validated against several crystallization experiments with good success[9].

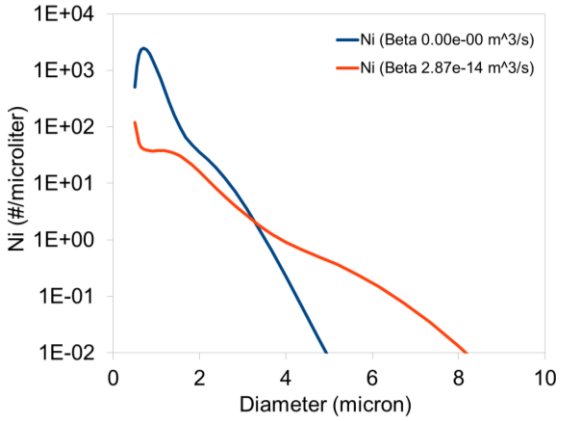

Figure 5. Volume integrated CaOx number density as function of diameter for non-agglomeration and agglomeration cases in the OMCD segment.

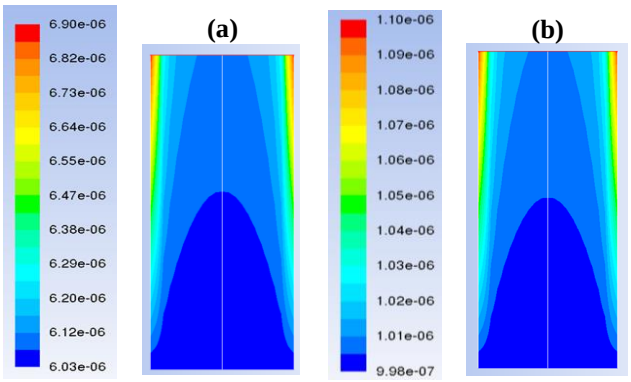

Figure 6. CaOx volume fraction distribution in the OMCD segment: (a) β = 0; (b) β = 2.5(10)$^{-14}$ m^3/s. Figure is not to scale.

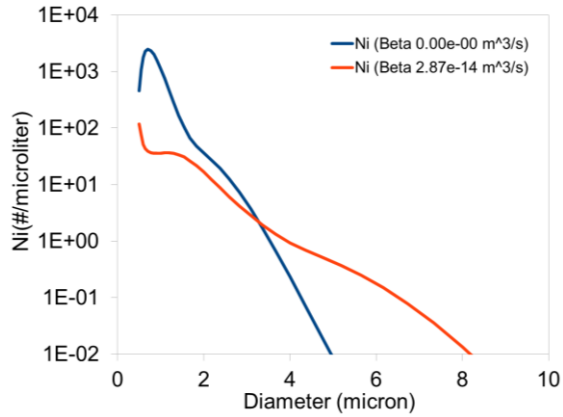

Figure 7. Volume integrated CaOx number density as function of diameter for non-agglomeration and agglomeration cases in the DoB segment.

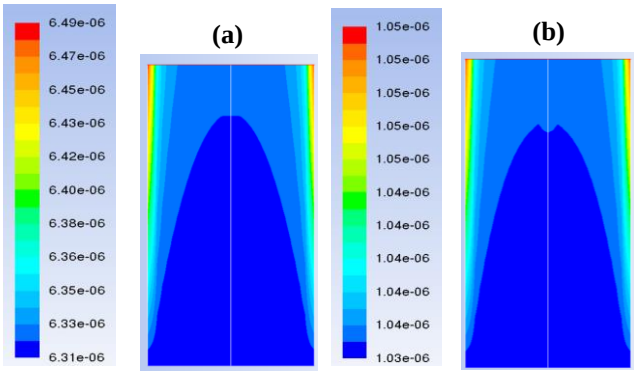

Figure 8. CaOx volume fraction distribution in the DoB segment: (a) β = 0; (b) β = 2.5(10)$^{-14}$ m^3/s. Figure is not to scale.

IV. Results and Discussion

As mentioned before, the numerical results presented here are based on urinary calcium and oxalate concentrations taken from an average of 86 urine samples taken from the astronauts on the day of landing[24] and the net urinary flow rates for each segment as listed in Table 1 as calculated by Kok and Kahn[15] based on a nominal 1.44 liter urinary excretion rate. To study renal stone development in microgravity, pseudo-transient simulations were performed and evolved to steady state for each nephron segment under weightlessness condition (g= 0). To underscore the important impact of agglomeration, both growth-only (non-agglomeration) and growth and agglomeration cases studies were performed.

We first look at the steady state distributions of stone number density, N_i, and stone volume fraction, α_2, in the tubule segment of the nephron. The volume averaged renal stone population density in the tubule section is presented both for the non-agglomeration case (only nucleation and growth with β = 0) and for the nucleation, growth, and agglomeration case with β = 2.5(10)$^{-14}$ m^3/s in Fig. 1. If we take the N_i = 0.01 #/microliter level as an arbitrary basis of comparison, we note that in the tubule section, the crystals have the potential to form and enlarge through nucleation and growth from a nidus size of 0.5 microns to a size of around 4 microns in diameter. For the non-agglomeration case, we note that the largest population of crystals occur at the nidus or nucleation size of 1.5 microns and then declines monotonically with larger crystal sizes. The results presented for the agglomeration case with β = 2.5(10)$^{-14}$ m^3/s indicates that the impact of agglomeration is considerable and has the potential to nearly double the largest stone size in the tubule segment. This enlargement is accomplished at the expense of the smaller calculi that agglomerate to

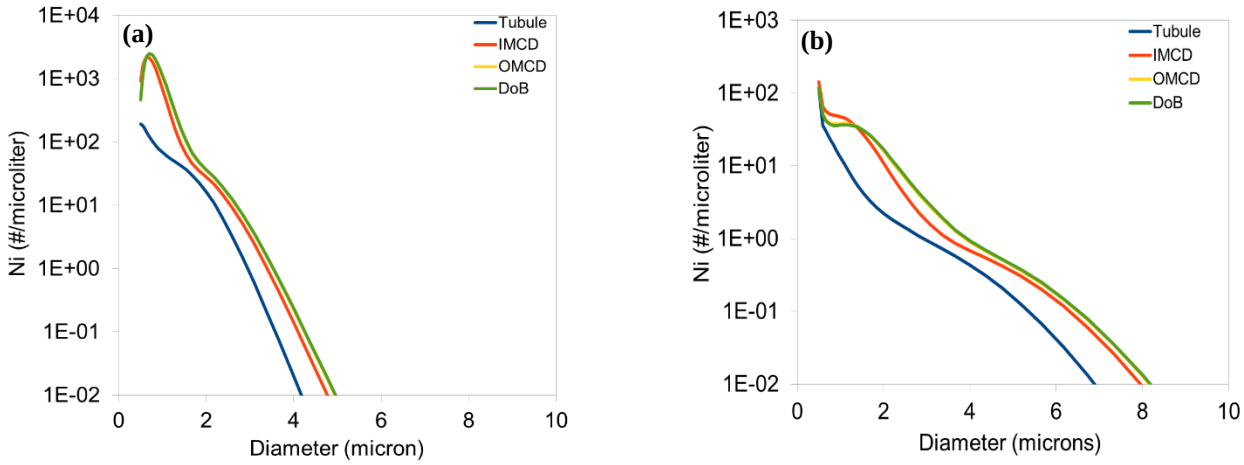

Figure 9. Log-Linear plot of the volume-integrated CaOx number density as function of diameter indicating maximum stone size in the 4 nephron segments: (a) $\beta = 0$; (b) $\beta = 2.5(10)^{-14}$ m^3/s.

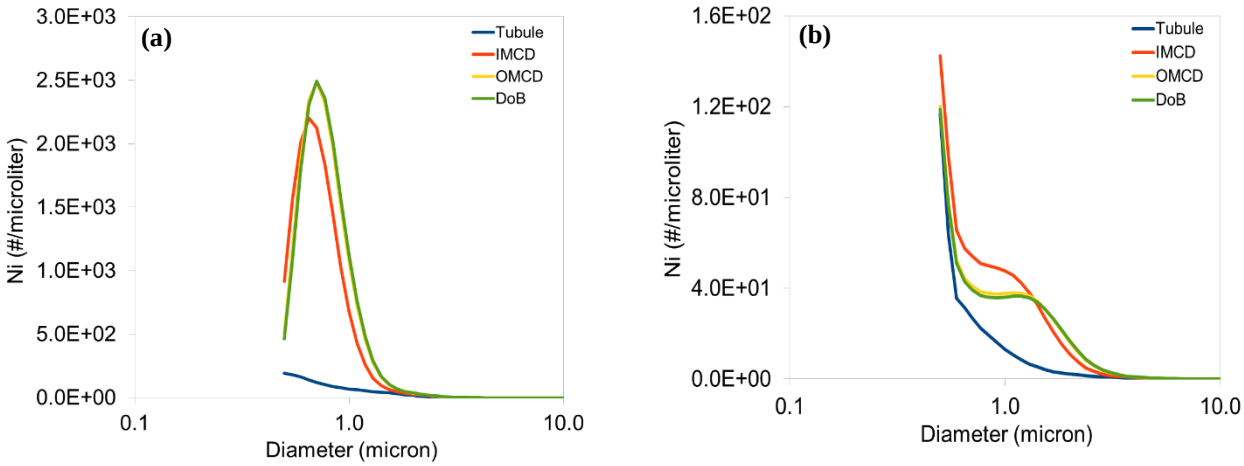

Figure 10. Linear-Log plot of volume-integrated CaOx number density as function of diameter indicating stone diameter at which peak number density occurs in the 4 nephron segments: (a) $\beta = 0$; (b) $\beta = 2.5(10)^{-14}$ m^3/s.

form the larger crystals. As a result, for the agglomeration case, the number of crystals in the smaller bins (below 3 microns) falls below those of the non-agglomeration case while the number of stones in the larger volume bins increase considerably over the growth only case.

The stone volume fraction distributions in the tubule section for the non-agglomeration and agglomeration cases are shown in Fig. 2a&b. The contours clearly indicate that the largest renal calculi volume fractions occur near the tubule wall where the urine velocity is lowest and thus the local transit times are the greatest. The thickness of the high volume fraction layer near the wall increases along the tubule length and is highest at the outlet. It is also interesting to note that the stone volume fraction level in the tubule is higher for the $\beta = 0$ case. In absence of agglomeration, there are more nucleates and small size crystals available to grow in size. Moreover in this case, the increase in renal calculi size occurs solely through addition of new mass from the urine supply that occurs over an increasing total effective growth surface area. However, when agglomeration is included, a significant portion of crystal enlargement takes place through adhesion of the smaller crystals to each other to form larger aggregates with a relatively smaller increase in the total effective surface area. As a result for $\beta = 2.5(10)^{-14}$ m^3/s case, the crystal enlargement occurs with a lower creation of new renal calculi mass from the urinary supply. Hence the volume fraction in the tubule is lower for the $\beta = 2.5(10)^{-14}$ m^3/s case compared to the $\beta = 0$ case although larger numbers of larger stone sizes are produced at the higher agglomeration rate.

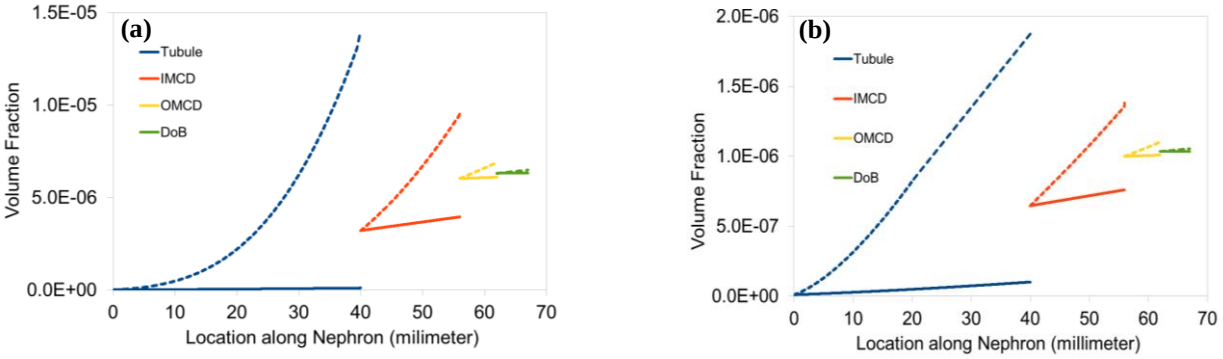

Figure 11. CaOx volume fraction as a function of distance along the nephron for: (a) $\beta = 0$; (b) $\beta = 2.5(10)^{-14}$ m^3/s. Solid line represent value at the conduit centerline and dahed line represents value at conduit wall.

The steady state stone number density and volume fraction for the IMCD, OMCD and DoB segments of the nephron are presented respectively in Figs 3-8. It is apparent that agglomeration is a major mechanism for renal stone size enhancement in all three duct segments. However note that while about 10-20% additional stone size increase occurs in the IMCD for both agglomerating and non-agglomeration cases, there is minimal further change in the size distributions as the calculi pass through the OMCD and DoB segments due to shorter duct lengths and faster transit times. This is clearly evident from a direct comparison of stone size distributions for the different nephron segments as shown respectively in Figs 9a and 9b for the non-agglomeration and agglomeration cases with the OMCD and DOB curves indistinguishable from each other. In Fig. 10a the stone number density is plotted against the log of stone diameter for the $\beta = 0$ case to show that there is a distinct peak in the stone number densities when growth is the main mechanism for size enhancement. The peak occurs at the nidus diameter for the tubule segment and moves towards a larger diameter of 1 micron for the OMCD and IMCD/DoB segments. A peak in the number density distribution is not observed for the $\beta = 2.5(10)^{-14}$ m^3/s case as shown in Fig. 10b where the largest population of crystals occur at the smallest nucleation size for all the nephron segments.

The volume fraction contours in the IMCD, OMCD, and duct of Bellini sections as shown in Figs 4, 6, and 8 display quite similar distributions with relatively higher volume fraction layers formed at the duct walls compared to the core flow region. However, notice that the maximum and minimum contour values approach each other as we progress from one duct section to the next, to the extent that the stone volume fraction distribution in the last segment, the DoB, becomes nearly uniform. This is also corroborated by comparing the line plots of volume fractions at the wall and at the centerline for the 4 segments as displayed respectively in Figs 11a and 11b for $\beta = 0$ and $\beta = 2.5(10)^{-14}$ m^3/s cases. Since the volume fraction at the entrance of each section is given by the area-averaged volume fraction at the exit of the previous section, the difference between the wall and centerline values diminish as we go from segment to segment.

The assumption of uniform volume fraction at the inlet of each nephron segment as adopted in the current analysis may not be too far from reality. The nephron consists of a cascading system of millions of interconnected tubules and ducts where in each branch of it, 6 tubules are connected to each OMCD, 39 OMCDs pour into to each IMCD, and finally 16 IMCDs enter a single duct of Bellini. It is assumed that the emergence of outflow from several conduits into the entrance of the next one involves mixing that creates a near uniform or well-mixed condition at the inlet of that conduit. From the results in Figs. 2, 4, 6, 8, and 11 it can be deduced that the tubule and IMCD sections are where most of the stone enlargement takes place. The largest normal gradient of volume fraction also form at the wall of these two segments. The OMCD and DoB segments seem to be where most of the mixing takes place ensued by relatively small size increase due to the rapid transit times. These two segments seem to uniformize the solid CaOx volume fraction in the ducts before they flow into the pelvis.

The average stone diameters at the conduit wall and conduit centerline are shown respectively in Figs 12 a&b for both agglomeration and no agglomeration cases. It is apparent that average stone size decreases near the wall and increases at the centerline as we proceed from segment to segment for both agglomerating and non-agglomerating cases as consistent with our previous mixing discussion. It is also interesting to note that the average stone size seems to be twice as large for the case with agglomeration (both at the wall and at the centerline) as compared to the non-agglomeration case.

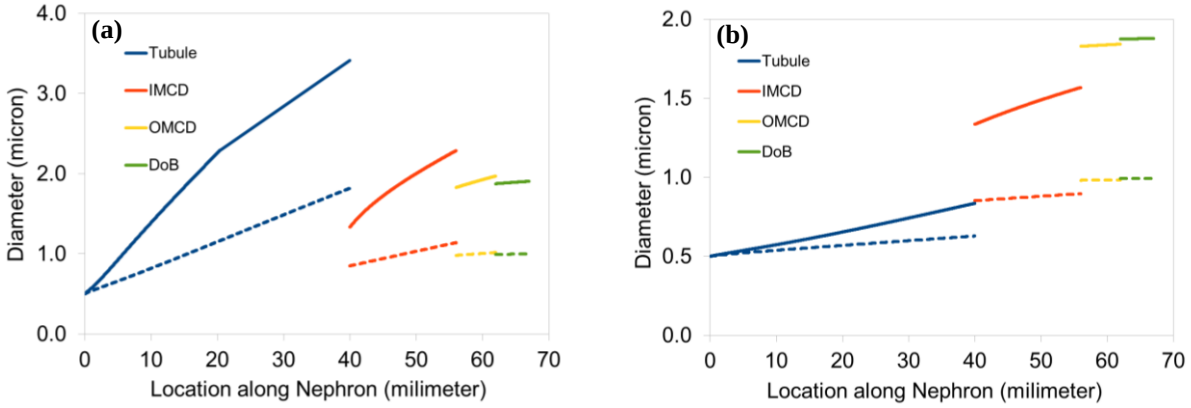

Figure 12. Mean CaOx diameter as function of distance along the nephron at: (a) conduit wall; (b) conduit centerline. Dashed line represent $\beta = 0$ case and solid line represents $\beta = 2.5(10)^{-14}$.

The centerline concentrations of calcium and oxalate along the nephron are presented respectively in Figs. 13 a&b for both agglomeration and non-agglomeration cases. It is interesting to note the depletion of bulk calcium and oxalate concentrations as renal calculi form while urine passes through the nephron. Notice that the urinary species depletion are much higher for the non-agglomeration case. As mentioned before, in the absence of agglomeration, all of the renal stone enlargement is due to growth. This case also has the largest effective surface area for deposition. However, with agglomeration, a large portion of size enhancement takes place by attachment of smaller crystals to form larger ones with a more limited increase in the effective surface area for precipitation. Therefore, for the agglomeration case, there is smaller net mass transfer of species from urine to stone and hence less urinary depletion as compared to growth only case. It is interesting to note that for the non-agglomeration case the largest depletion of Ca and Ox takes place in the IMCD segment.

Finally, our numerical results predict that the largest stone sizes that are produced in the nephron under microgravity conditions due to simultaneous growth and agglomeration will be still considerably below the critical size of 50-100 microns for direct duct blockage. However, note that with the larger volume fractions near the tubule and duct walls especially in the IMCD there is an increased potential for wall adhesion and subsequent development towards a critical size.

V. Conclusion

A deterministic model was presented to assess the risk of critical renal stone formation for astronauts during space travel. The model was developed by coupling the PBE for nucleating, growing and agglomerating renal calculi to a CFD model that solves for flow of urine, conservation of species, and transport of renal calculi in the nephron using a Eulerian two-phase mathematical framework.

Parametric simulations were performed to study steady state stone size and volume fraction distributions in the four main sections of the nephron under weightlessness conditions. Results indicated that agglomeration has a profound effect on the renal stone size distributions by decreasing the population of smaller stones and increasing the number and sizes of the larger stones in all four segments of the nephron. It was found that due to the retarding effect of the wall on the urinary flow the volume fraction of the stones is dramatically increased at the walls of tubule and IMCD segments. Thus for these first two nephron segments, a mixed-suspension mixed-product removal (MSMPR) continuous crystallizer model as adopted by many of the previous theoretical work is not valid.

Our numerical results further show that mixing due to the cascading transition between the nephron segments produces quite uniform volume fraction distributions in the DoB. Simulations using measured astronaut urinary calcium and oxalate concentrations in microgravity as input indicate that under nominal conditions the largest stone sizes developed in Space will be still considerably below the critical range for problematic stone development. However, our results also indicate that since the highest stone volume fraction occurs next to the tubule and duct walls, there may be an increased propensity for wall adhesion with a possible risk of evolution towards critical sizes. More detailed CFD models that can rigorously capture the urine-crystal-wall interactions are needed to provide a deeper understanding of critical renal stone formation.

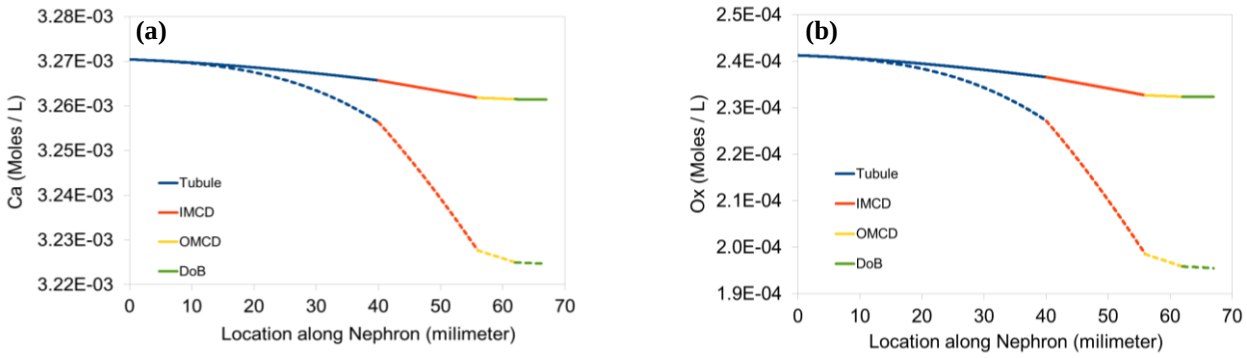

Figure 13. Centerline Ca (a) and Ox (b) concentrations as a function of distance along the nephron: dashed line represent $\beta = 0$ case and solid line represents $\beta = 2.5(10)^{-14}$ case.

Acknowledgments

We gratefully acknowledge funding support from the Exploration Medical Capabilities Element of NASA's Human Research. Many thanks also goes to Drs. DeVon Griffin and Jerry Myers from NASA Glenn Research Center (GRC) and Dr. Robert Pietrzyk from NASA Johnson Space Center (JSC) for their constant support and valuable advice.

References

[1]Pietrzyk, R.A., J.A. Jones, C.F. Sams, P.A. Whitson, Renal stone formation among astronauts. Aviation Space and Environment Medicine. 78 (4) Section II: A9-A13, 2007.

[2]Sibonga, J.D., Evidence book: risk of renal stone formation. National Aeronautics and Space Administration, London B. Johnson Center Houston TX, HRP-47060, 2008.

[3]Jones, A.J. , R.A. Pietrzyk, A. Whitson, Renal & genitourinary concerns, in: M.R. Barrat, S.L. Pool (Eds.), Principals of Clinical Medicine for Space Flights, Springer NY, 2008, 273-292.

[4]Watenpaugh, D.E., Fluid volume control during short-term space flight and implications for human performance, J. Exp Biol, 204(9):3209-3215, 2001.

[5]Whitson, P.A., R.A. Pietrzyk, C.F. Sams, Urine volume and its effects on renal stone risk in astronauts, Aviation Space and Environment Medicine. 72(4):368-372, 2001.

[6]Zerwekh, J.E, Nutrition and renal stone disease in space, Nutrition, 18:854-863, 2002.

[7]Whitson, P.A., R.A. Pietrzyk, J.A. Jones, M. Nelman-Gonzales, Effect of potassium citrate therapy on the risk of renal stone formation during spaceflight, J. Urology, 182:2490-2496, 2009.

[8]Stamatelatos, M., H. Dezfuli, Probabilistic risk assessment procedures guide for NASA managers and practitioners, NASA/SP-2011-3421, Second Edition, NASA Headquarters, Washington, DC, 2011.

[9]Kassemi, M., D. Thompson. Prediction of Renal Stone Size Distributions in Microgravity Using a PBE Analytical Model: 1. Effect of Space-Induced Biochemical Alterations, Anal of Biomedical Engineering. Submitted (2015).

[10]Kassemi, M., M., Brock, R, Nemeth, N., A combined transport, kinetics model for the growth of renal calculi, J. Crystal Growth, 332(1):48-57, 2011.

[11]Nielsen, A.E., J. Christofferesen, The mechanisms of crystal growth and dissolution. In: Biological Mineralization and Demineralization, edited by G.H. Nancollas, Dehlem Konferenzen. Berlin, Heidelberg, New York, Springer-Verlag, 1982, pp 37-77.

[12]Finlayson, B., The concept of continuous crystallizer: its theory and application to in-vivo and in-vitro urinary tract models, Invest. Urol, 9(4):258-262, 1972.

[13]Finlayson, B., F. Reid, The expectation of free and fixed particles in urinary stone disease, Invest. Urol., 15(6):442-448, 1978.

[14]Kavanagh, J.P., Methods for the study of calcium oxalate crystallization and their application to urolithiasis. Research, Scanning Microsc. 6:685-705, 1992.

[15]Kok, D.J., S.R. Khan SR, Calcium Oxalate nephrolithiasis, a free or fixed particle disease. Kidney Int. J., 46:847-854, 1994.

[16]Robertson, W.G., Kidney models of calcium oxalate stone formation, Nephron Physiol, 98:21-30, 2004.

[17]Kim, S.C, et al., Stone formation is proportional to papillary surface coverage by Randall's plaque, J. Urology, 173:117-119, 2005.

[18]Evan, A.P., Worcester, E.M., Coe, F.L., Williams, J., Lingerman, J.E., Urolithiasis, Mechanisms of Human Kidney Stone Formation, 43(1):19-32, 2015.

[19]Hounslow, M. J., A discretized population balance for continuous systems at steady state, AICHE J., 36: 106-116, 1990.

[20]Randolph. A.D., M.A. Larson, Theory of Particulate Processes, Academic Press, San Diego, 1988.
[21]ANSYS Fluent Documentation. Release 13.0. November 2010.
[22]Borissova, A., G.E. Goltz, J.P. Kavanagh, T.A. Wilkins, Reverse engineering the kidney: modelling calcium oxalate monohydrate crystallization in the nephron, Med Biol. Eng. Comput., 48:649–659, 2010.
[23]Zauner, R., A. G. Jones, Determination of nucleation, growth, agglomeration, and disruption kinetics from experimental precipitation data: the calcium oxalate system. Chemical Engineering Science, 55:4219-4232, 2000.
[24]Whitson, P.A., R.A. Pietrzyk, C.Y.C Pak, N M. Cintron, Alterations in renal stone risk factor after space flight, J. of Urology, 150:803-807, 1993.
[25]M. J. Hounslow, R. L. Ryall, and V. R. Marshall. *"A Discretized Population Balance for Nucleation, Growth, and Aggregation"*. *AIChE Journal*. 34(11). 1821–1832. 1988.
[26]J. D.Litster, D. J.Smit, and M. J.Hounslow. "Adjustable Discretization Population Balance for Growth and Aggregation". AIChE Journal. 41(3). 591–603. 1995.
[27]Meyer, J.L., L.H. Smith, Growth of calcium oxalate crystals: II. Inhibition by natural urinary crystal growth inhibitors, Invest. Urol. 13(1):36-39, 1975.
[28]R. Burton-Optiz, R. Dinegar, The Viscosity of Urine, Am. J. Physiol 74 (1918) 220-230.
[29]A.E. Nielsen, Transport Control in Crystal Growth from Solution, CCACCA 53 (2) (1980) 255-279.